

PAPER • OPEN ACCESS

Feasibility of ultra-compact HTS CrossConductor based Power Transmission Cables

To cite this article: Dustin Kottonau *et al* 2020 *J. Phys.: Conf. Ser.* **1559** 012084

View the [article online](#) for updates and enhancements.



IOP | ebooks™

Bringing together innovative digital publishing with leading authors from the global scientific community.

Start exploring the collection—download the first chapter of every title for free.

Feasibility of ultra-compact HTS CrossConductor based Power Transmission Cables

Dustin Kottonau¹, Michael Wolf¹, Walter Fietz¹, Jörg Stammen², Holger Hirsch²

¹ Karlsruhe Institute of Technology, Germany

² University of Duisburg-Essen, Germany

E-mail: dustin.kottonau@kit.edu

Abstract. HTS CrossConductor is a compact stacked-tape REBCO conductor of high current density. In this contribution, a non-concentric three-phase cable design based on HTS CroCos is presented, which offers the possibility to reduce the cable diameter significantly. One of the important aspects of HTS-AC power cables are the AC-losses, which are investigated both theoretically and experimentally. For the measurement of the dissipated power loss in both single-phase and three-phase conductor arrangements, a calorimetric method is used. The results indicate that it is possible to reduce the outer cable diameter compared to concentric cables designs by a factor of two. When the losses of such a cable with HTS CroCo design shall not exceed 2 W/m for all three-phases, the maximum ampacity results in a current of 600 A(rms) per phase. Depending of the target there are many potential applications for such an ultra-compact HTS CroCo-based power transmission cable design.

1. Motivation

Numerous feasibility studies [1] reveal that so-called “retrofitting” of conventional cable systems will be an important application of superconducting cable systems in future. If a conventional cable system reaches the end of its service life, the distribution grid operator mostly faces the challenge of replacing it by a system of higher current carrying capacity in the existing infrastructure, called retrofit. The re-use of existing infrastructure, for example protective tubes, is economically advantageous in any case.

Due to their high current carrying capacity, superconducting cables are predestined for this application. When constructing and designing superconducting cables, compact cable diameters are among the most important requirements to be met in urban areas.

Classical superconducting cable concepts, such as the three-phase concentric cable as used in the Ampacity project, have relatively large outer cable diameters of about 150 mm [2]. This is due to the concentric, layered structure of the cable and the relatively large inner tube diameter.

Since 2016, KIT’s Institute for Technical Physics has been working on the so-called “HTS CrossConductor” concept [3]. The name “HTS CrossConductor” refers to the conductor’s cross-shaped design, where HTS tapes of two different widths are stacked in a cross-shaped fashion to form a conductor with high current density. Thanks to this design, rather compact conductor dimensions can be reached compared to concentric layers.

The present study deals with the principle applicability of this conductor concept for three-phase alternating current systems. It will concentrate in particular on the power loss of the cable concept. Power loss largely determines practical applicability of the new conductor type. The study will not cover the design of electrical insulation, the cooling concept, and other cable system components.



2. CrossConductor concept

The “CrossConductor” concept refers to a special arrangement of HTS stacked-tape conductors. The design is aimed at reaching a maximum current carrying capacity within a circular conductor area. The circular cross-section conductor can be filled with commercially available, flat rectangular REBCO tapes. When stacking tapes of a single width in a round cross-section, the maximum filling factor is obtained for a square with a filling factor of 0.636. By adding another rectangular tape stacks of a smaller width on the upper and lower sides of the first rectangular stack, the so-called CrossConductor (CroCo) is obtained. This arrangement improves the filling factor of the conductor to 0.787 [3]. The increase of the filling factor results in a higher current density of the conductor.

The set-up and properties of the superconducting tape conductors and of the CrossConductor will be described in the following sections.

2.1. Set-up

The main components of the CrossConductor are the superconducting tape conductors, additional copper stabilisers between the superconducting tape, solder layers, and the solder shell. A detailed set-up of the CrossConductor is shown in Figure 1.

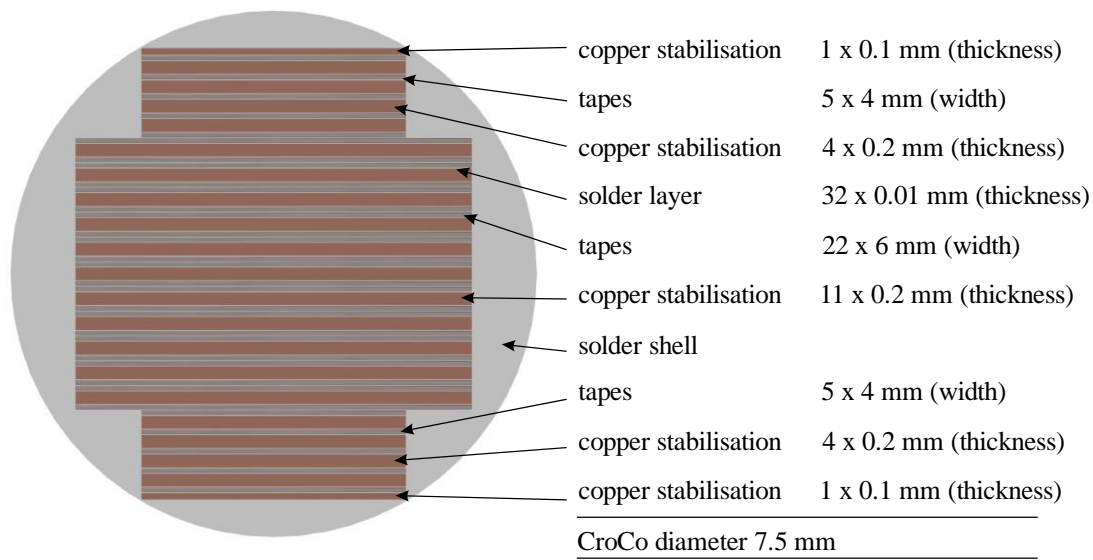


Figure 1. Schematic overview of the CrossConductor set-up and dimensions of the layers.

2.1.1. Superconducting tape conductors. The CrossConductor is made of superconducting tape conductors manufactured by Shanghai SC with a copper stabilisation thickness of 50 μm . For manufacturing reasons, distribution of critical current varies over the length of the tape conductor. For a tape conductor of 4 mm width, a mean value of 130 A is assumed. The tape conductor of 6 mm width is assumed to reach a mean value of 210 A. Percentage deviation of the min-max value of the 4 mm tape conductor is 11.4%, while that of the 6 mm tape conductor amounts to 8.4% [4].

For a theoretical estimation of AC losses, the critical current I_{C0} is converted into the critical current density j_{C0} . Considering the width b and height h of the superconducting layer and the critical current, current density can be calculated as follows [5]:

$$j_{C0} = \frac{I_{C0}}{A} = \frac{I_{C0}}{h \cdot b} \quad (1)$$

For a superconducting layer thickness of 1 μm [6], the critical current density is $3.3\text{e}+11$ A/m² taking into account the variation of critical current.

2.1.2. Copper stabilisation between the tape conductors. The additional copper stabilisation serves to thermally stabilise the tape conductors in the case of overcurrent and subsequent quench. Part of the overcurrent is distributed over the copper stabilisation and the superconducting layer is protected against overload. The copper stabilisation also ensures low-resistance transition between the superconducting tape conductors and power supply [7].

2.1.3. Solder layer/solder shell. The tape conductors and copper stabilisers are connected by soldering in a solder bath. Then, they are enclosed by a spherical solder shell.

2.2. Resulting critical currents

Calculation is made using the magnetostatics option in the electromagnetic module of the finite element method in COMSOL. Taking into account the fluctuating critical current, a minimum value of 3240 A results for the total current. The mean value is 3520 A, the maximum is 3840 A in agreement with conductors of the same geometry used for a DC cable demonstrator [4].

3. CrossConductor - Cable concepts

A superconducting cable system consists of cables, fittings, a refrigeration system, and secondary technology. The superconducting cable is divided into the cable core and cable cryostat. The cable cryostat is used as thermal insulation and may be of rigid or flexible design. Hence, the cable cryostat is an important design parameter when realising a superconducting power cable [8]. The cable cryostat consists of the inner and outer cryostat tubes, the so-called superinsulation with an evacuated gap, and a polyethylene enclosure of the outer cryostat tube.

Figure 2 schematically represents a flexible cable cryostat with its components and the potential three-phase arrangement of the CrossConductor.

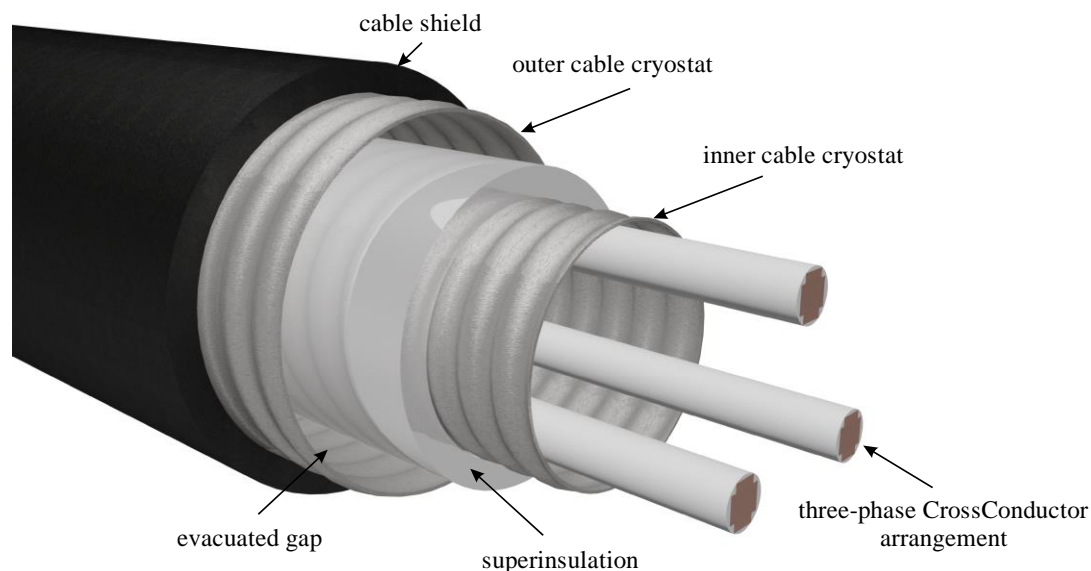


Figure 2. Schematic representation of a flexible cable cryostat, its components, and potential three-phase arrangement of the CrossConductor.

The inner cryostat diameter is of crucial importance to the cable design. Its available cross-section determines the thermal and hydraulic design limits. This helps to assess technical feasibility of a planned transmission line[1]. Here, standardised diameters of DN 40, DN 50, and DN 65 are assumed [9]. Arrangement of a three-phase conductor system (true-to-scale) as a function of the distance is represented in Figure 3.

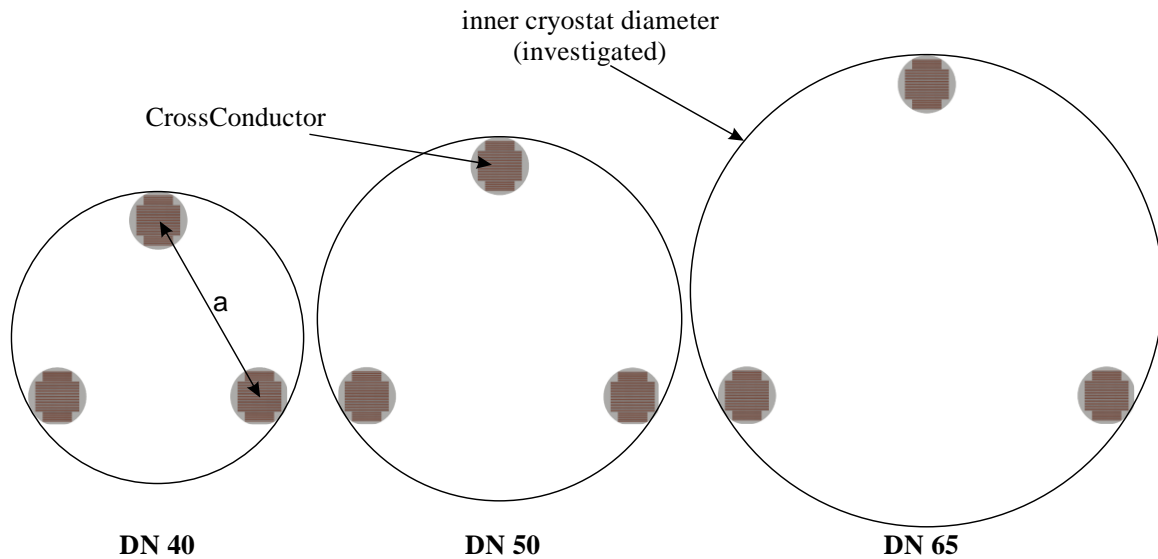


Figure 3. Arrangement of a three-phase conductor system (true-to-scale) as a function of the distance a .

To estimate the outer cable diameter, the thickness of the thermal insulation, the outer cryostat and the cable shield has to be added [1]. Therefore, the calculated outer cable diameter results at DN 65 in 114 mm, at DN 50 in 94 mm and at DN 40 in 78mm. Compared to concentric cable design, at minimum DN 80 is 150 mm [1], the outer cable diameter is smaller by the factor of 2. The design of electrical insulation, the cooling concept, and other cable system components are not examined here.

4. CrossConductor – Calculated AC losses

Hysteresis losses can be modelled using two simplified analytical models. The first model simulates the CrossConductor by a single tape conductor. In the second model, the CrossConductor is considered to be a round or elliptical conductor. Both models serve to determine the loss range in the sense of a best-case and worst-case estimation [10].

To estimate hysteresis losses P_D of an infinitely thin single tape conductor, Equation 2 is used [11]. The AC losses are depending on the critical current of the CrossConductors I_C , the load factor F and the network frequency f_N (in Germany 50 Hz). It is assumed that the magnetic field is limited to two points at the edge of the superconducting layer. In the field-free space between these edge points, no losses are produced.

$$P_D = \frac{\mu_0 \cdot I_C^2}{\pi} \cdot f_N \cdot [(1 - F)\ln(1 - F) + (1 + F)\ln(1 + F) - F^2] \quad (2)$$

A simple model to estimate hysteresis losses of elliptically shaped tape conductors P_E is approximation equation 3 [11]. The “inner” stack structure of the CrossConductor (CroCo) is not considered in detail, but to be bulk material. The alternating field applied produces more losses in the elliptical cross-section than in the infinitely thin tape conductor layers.

$$P_E = \frac{\mu_0 \cdot I_C^2}{\pi} \cdot f_N \cdot \left[(1 - F)\ln(1 - F) + (2 - F) \cdot \frac{F}{2} \right] \quad (3)$$

Figure 4 shows the power losses of the two theoretical models. With increasing conductor current, AC losses increase considerably. At a conductor current of 1000 A(rms), the specific single-phase power loss amounts to about 3 W.

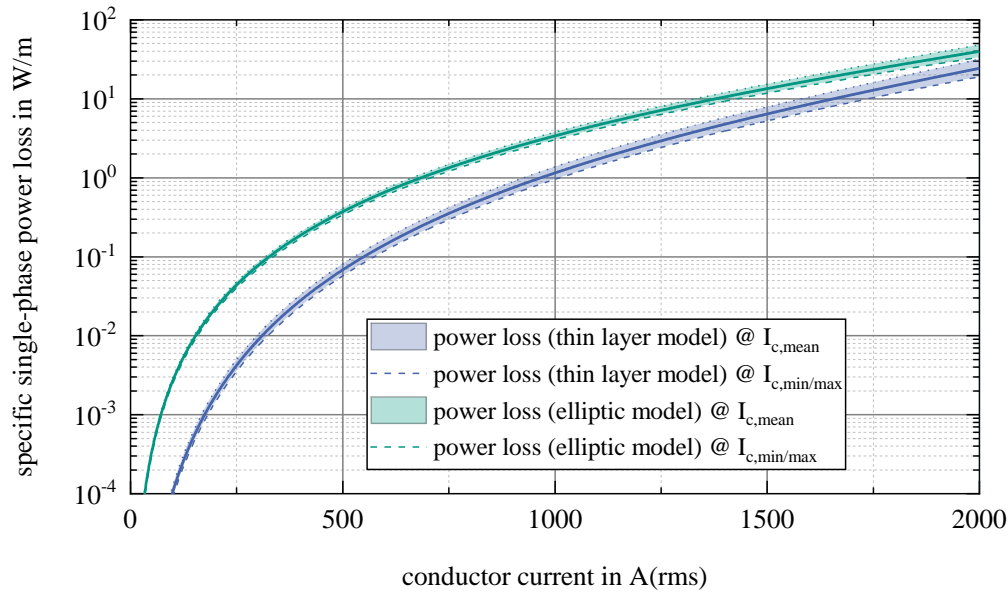


Figure 4. Power losses of the three conductor models as a function of the conductor current.

5. Laboratory set-up

The test set-up consists of three main components, a variable transformer, a high-current transformer, and a cryostat. The variable transformer is used to control voltage. With the help of the high-current transformer, the currents required for the test (> 1 kA) are produced. The cryostat contains the CroCo segments cooled with liquid nitrogen. Each of these components is of modular design. All interfaces of these modules are designed as plug connections. This results in two advantages. Firstly, modular design facilitates planning and construction. Secondly, the fabricated modules can be arranged easily depending on the set-up. With the help of a lift truck, the modules fixed on euro pallets can be positioned, transported, and stored easily. Figure 5 presents a schematic overview of the main components and their interfaces.

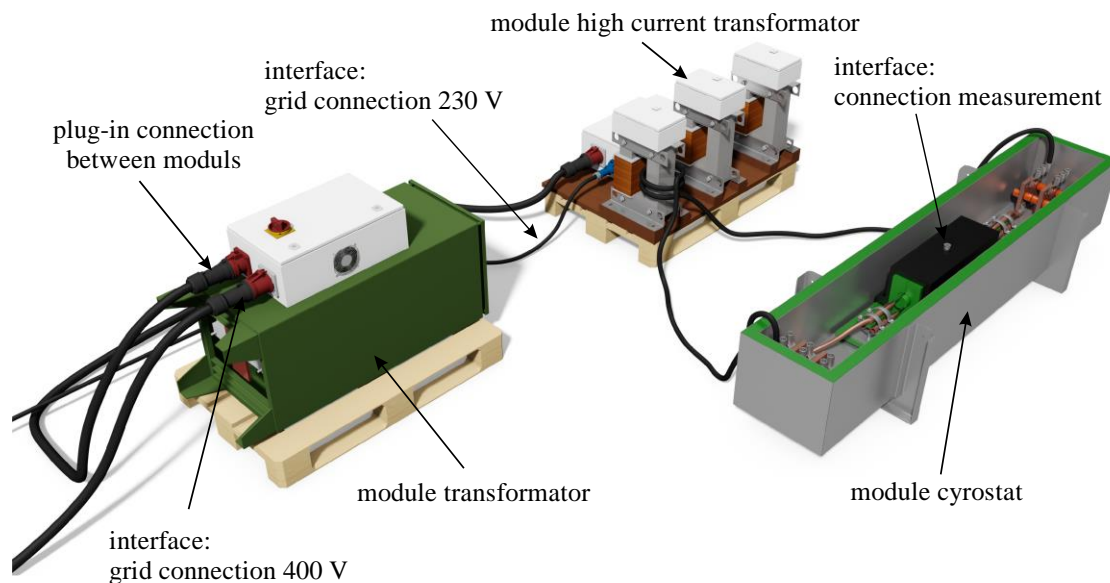


Figure 5. Schematic overview of the single-phase test set-up and its modules.

5.1. Variable transformer module

The variable transformer module is supplied with power via a three-phase mains connection. Using the screw drive of the variable transformer, an output voltage of 10 – 400 V (conductor-conductor voltage) can be set. An electrically locked change-over switch controls the screw drive. Fine adjustment is limited by a voltage of 1 V/step. The rated current of the variable transformer amounts to 50 A.

5.2. High-current transformer module

The high-current transformer module is connected to the variable voltage output of the variable transformer module. With the transformer ratio of 1:80, a secondary current of 20 – 2900 A is generated. The module can be switched between single-phase and three-phase operation using the motor terminal boards. Fine adjustment of the transformer ratio is made with the auxiliary winding of the primary windings of the high-current transformers.

5.3. Cryostat module

The cryostat consists of two current leads and the measurement chamber for loss measurement of the CroCo segments. In operation, the 2.5 m long cryostat is filled with 200 – 250 l of liquid nitrogen. At a filling level of 300 mm, the current leads and the measurement chamber are completely covered by nitrogen.

5.3.1. Measurement chamber. The measurement chamber collects the evaporating nitrogen for volume flow measurement. On the inner surface, the lid of the measurement chamber is shaped like a funnel to prevent uncontrolled accumulation of nitrogen in a corner of the chamber. To keep the filling level of liquid nitrogen in the measurement chamber constant, nitrogen supplies are integrated in the bottom of the chamber. The measurement chamber is made of highly dense polyethylene (HD-PE-300). This material is cheaper than glass-fibre reinforced plastic and suited well for the manufacture of complex designs of large-volume structures in one piece.

5.3.2. Guiding rod. With the help of guiding rods, the distances between the CroCo segments can be adjusted (DN 40, DN 50, and DN 65). In this way, a dimensional accuracy of ± 0.3 mm is ensured. Four recesses along the guiding rod prevent the evaporating nitrogen from accumulating in the two lower

guiding grooves and influencing the volume flow measurement. Due to the forces occurring between the CroCo segments, the guiding rods are made of glass-fibre reinforced plastic (EP GC 201).

5.3.3. End cap. To seal the measurement chamber and to prevent the evaporating nitrogen from escaping laterally, end caps are used for the three diameters to be studied (DN 40, DN 50, and DN 65). To ensure that thermal shrinkage of the end caps and guiding rod is the same, glass-fibre reinforced plastic (EP GC 201) is used.

5.3.4. Gas outlet. The gas outlet is the interface between measurement chamber and measurement system. The downstream corrugated pipe is connected to the gas outlet via a small flange (ISO-KF-25).

5.3.5. Connector, spacer, pipe, clamps. The unit of connector, spacer, and pipe clamps is used as the transition piece between the copper conductor and the CroCo segments. This unit is not fixed to the base plate. Thermal length variations can be compensated. A schematic representation of the cryostat module with the current lead and measurement chamber is shown in Figure 6.

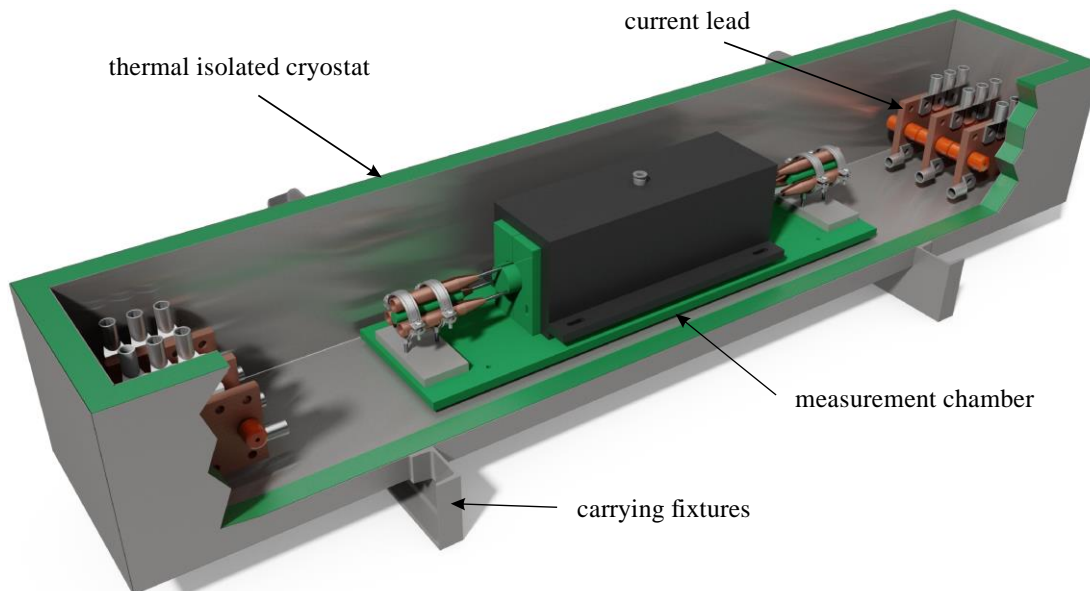


Figure 6. Schematic representation of the cryostat module with power supply and measurement chamber.

6. Experimental studies and results

Experimental studies include the measurement of critical current, calibration of loss measurement, and determination of AC losses of the single-phase and three-phase designs. Studies are completed by AC loss measurement with a corrugated stainless steel pipe.

6.1. Measurement of critical current

To theoretically estimate the AC losses, the critical current of the CroCo segment is required. In the “Resulting critical currents” section, this critical current was determined using computer-based field calculation. Here, the critical currents are verified experimentally in each of the three conductor segments. Critical current is measured by classical current-voltage measurement over a defined conductor distance.

The voltage curves recorded for each of the three CroCo segments reveal critical currents between 3,355 A and 3,413 A when using the IC criterion. Hence, the calculated and measured critical currents are in good agreement.

6.2. Calibration of loss measurement

Losses in the measurement chamber, i.e. AC losses of the CroCo segments are determined from the volume flow of evaporating nitrogen. For this, a correlation between defined power loss and volume flow is derived (calibration).

6.2.1. Measurement principle. For a clear correlation between power loss and the generated volume flow (calibration), power loss must be determined as precisely as possible. Voltage drop is measured over a defined DC resistance which is located in the liquid nitrogen under the funnel of the measurement chamber. With the help of Ohm's Law, the power loss dissipated in the DC resistance can be calculated, while the gas flow is determined that is produced by this dissipated power.

6.2.2. Results. The relationship between power loss and normalised volume flow is shown by the regression analysis in Figure 7. Apart from the regression function, measurement uncertainty and data points are indicated. Measurement uncertainty of the volume flow sensor is $\pm 1\%$ of the measurement range. Because the flow sensor is used with a maximum measurement range of 10 standard litres pro minute (SLPM), measurement uncertainty is 0.1 SLPM. This measurement uncertainty was added to the results of calibration in Figure 7 and results in the dashed lines.

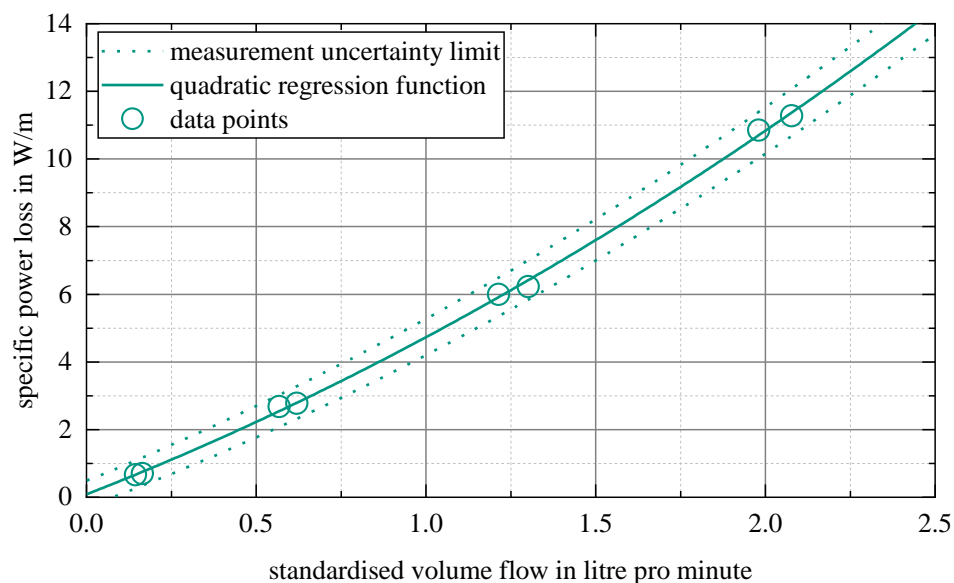


Figure 7. Specific power loss as a function of normalised volume flow.

As expected, volume flow increases about linearly with increasing losses. For example, specific power loss doubles when the normalised volume flow is doubled. It can also be noticed that the data points measured are in good agreement with the regression function used.

6.3. AC losses of the single-phase conductor set-up

With the help of the correlation determined between normalised volume flow and specific power loss (calibration of loss measurement), the AC current losses of the single-phase set-up are determined for each electrical phase (L1, L2, and L3).

6.3.1. Measurement principle. Measurements and data evaluation in this section are aimed at determining the relationship between the measured AC current and the normalised volume flow. By using the relationship described and the calibration derived in the previous section (calibration of loss

measurement), a relationship between the specific power loss and AC current is obtained. The result is then compared with the theoretical estimations of Figure 4.

6.3.2. *Results.* The specific power loss is plotted as a function of the conductor current of the single-phase set-up in Figure 8. The regression function, measurement uncertainty, and the data points are indicated. To study potential deviations of AC losses of the three CroCo segments, regression functions are generated for all three electrical phases (L1, L2, and L3).

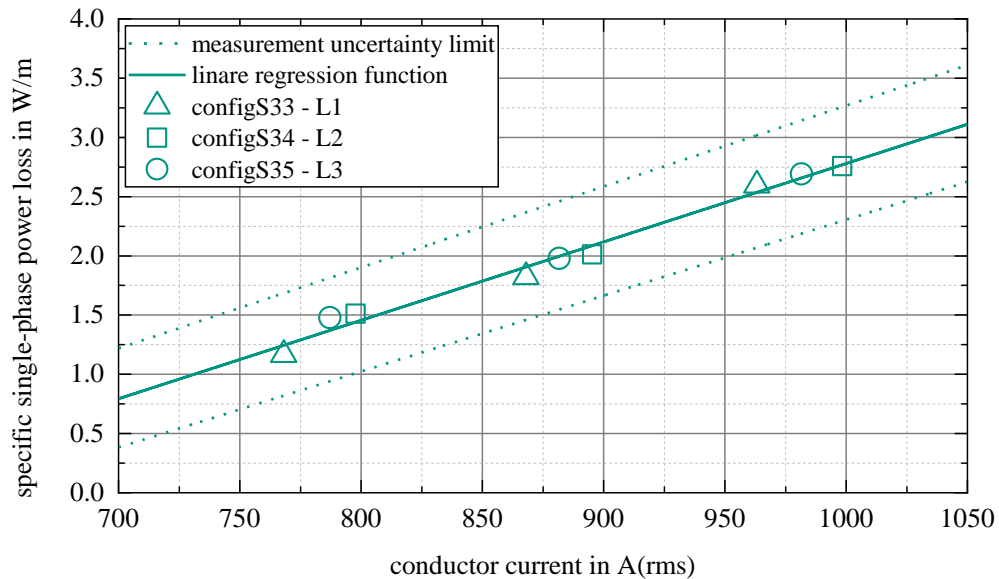


Figure 8. Specific power loss as a function of conductor current for the single-phase set-up.

At a conductor current of 760 – 1000 A(rms), specific single-phase power loss amounts to about 1.2 – 2.7 W/m. No significant differences of AC losses of the three different CroCo segments L1, L2, and L3 are found.

6.3.3. *Comparison of theory and experiment.* Here, the theoretical estimates of Figure 4 are compared with the data points measured. Theoretical and experimental specific power losses of the single-phase set-up are compared in Figure 9.

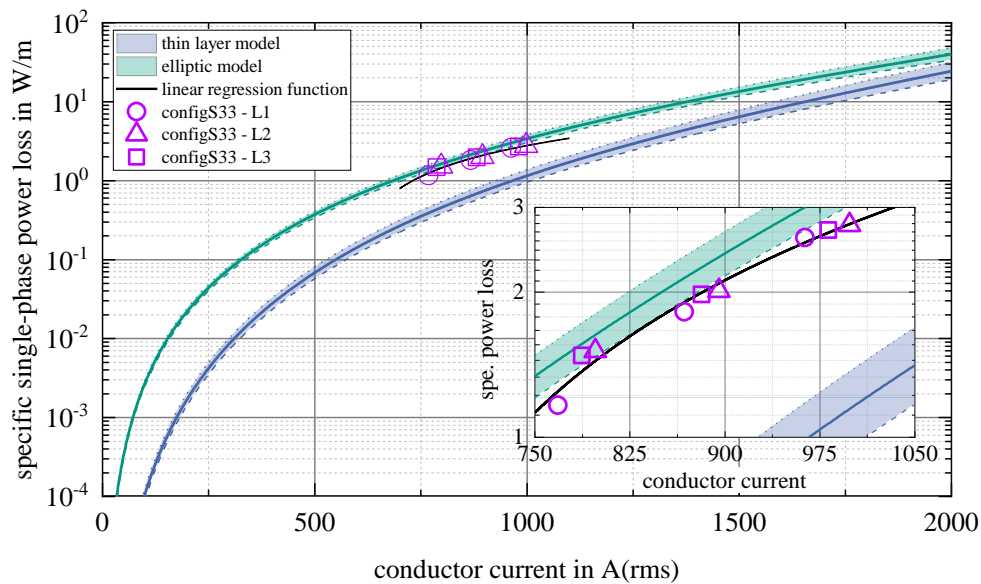


Figure 9. Comparison of theoretical and experimental specific single-phase power losses.

It is obvious from Figure 9 that AC losses of the CroCo segments range between the best-case and worst-case estimations, but much closer to the estimated loss of the elliptic model (worst case). Single-phase AC loss amounts to about 2.1 W/m at 900 A. This value will be used as a reference value for the three-phase set-up discussed below.

6.4. AC losses of the three-phase set-up

As in case of the single-phase set-up, AC losses of the three-phase CroCo set-up are also determined using the calibration. The measurement principle and process are the same and, hence, will not be discussed in detail here. To study the influence of the distances between the conductors, the AC losses are measured for three distances (DN 40, DN 50, DN 65; see Figure 3).

6.4.1. Results. The specific three-phase power loss is represented as a function of the conductor current for the three-phase set-up in Figure 10.

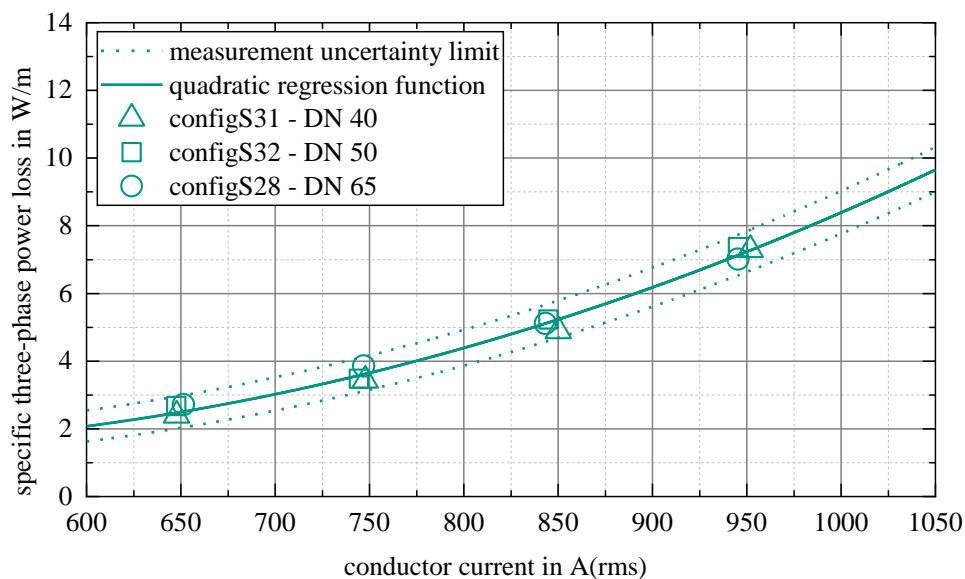


Figure 10. Specific three-phase loss as a function of conductor current for the three-phase set-up.

At a conductor current ranging from 650 – 950 A(rms), the specific three-phase power loss amounts to about 2.5 – 7.5 W/m. Figure 10 shows, that the influence of the cryostat diameter is small and due to the measurement uncertainties no clear correlation between power loss and cryostat diameter can be deduced. This implies, that the electromagnetic fields at the currents and conductor distance used are too small to reduce critical current or strongly increase the AC losses.

6.4.2. *Comparison of theory and experiment.* Figure 11 compares the theoretical and experimental specific single-phase power losses for the three-phase set-up.

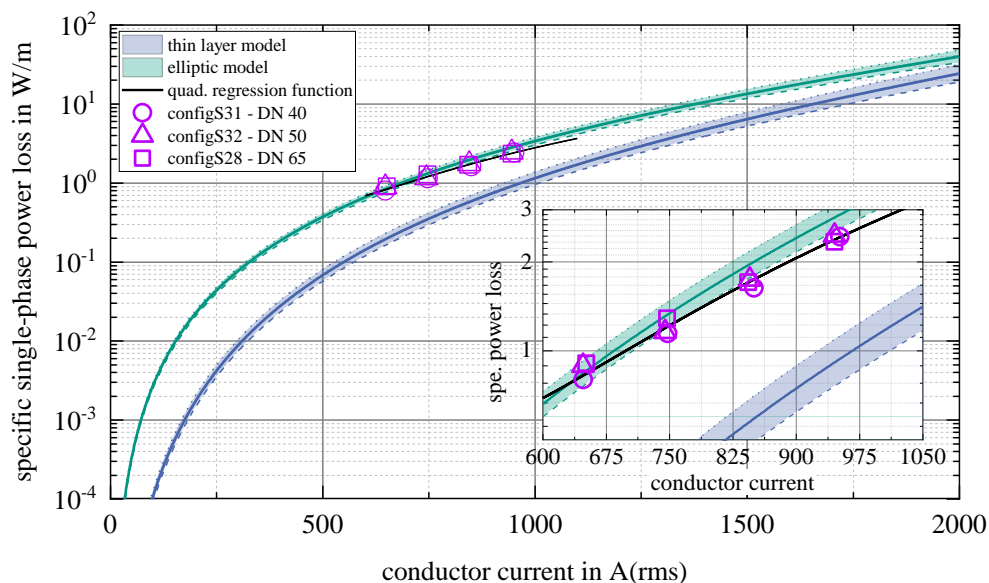


Figure 11. Comparison of theoretical and experimental specific single-phase power losses for the three-phase set-up.

As observed for the single-phase set-up, the data points measured are close to the worst-case loss model. For the measured current range, the elliptic loss model can be used for estimations with sufficient accuracy.

Single-phase specific AC loss for the three-phase conductor set-up amounts to about 2.1 W/m at 900 A. When comparing the losses of the single-phase and three-phase set-ups, no influence is found within measurement uncertainty. The three-phase CroCo set-up behaves linearly to the sum of the single-phase power losses of Figure 8.

The classical three-phase concentric cable concept (see “Ampacity”) has a power loss of about 2 W/m at a nominal current of 2.3 kA [2]. The same power loss is obtained for the three phase CroCo cable at a conductor current of 600 A(rms). Hence, if the allowable losses are fixed to 2 W/m. The permissible conductor current is smaller by a factor of approximately 4 in comparison to the classical concentric cable design.

6.5. AC losses of the three-phase set-up with a corrugated pipe

Here, the influence of the corrugated pipe on power loss shall be determined. For this purpose, the three-phase CroCo set-up is enclosed by a cryostat pipe (corrugated stainless steel pipe) of DN 50 in diameter. The electromagnetic fields of the CroCo conductors induce eddy currents in the surrounding corrugated stainless steel pipe. The resulting additional losses increase the volume flow of evaporating nitrogen. The sum of AC and eddy current losses is determined using the known relationship between normalised volume flow and power loss. The measurement principle and process of AC measurements are identical with those of the single-phase set-up.

The results shown that use of a corrugated pipe increases the specific power loss by about 1 W/m compared to the three-phase set-up without a corrugated pipe. At high conductor currents ($I_{AC} > 1,000$ A), the additional impact of eddy current losses should be considered.

7. Summary

The set-up used for the calorimetric measurement produces sufficiently precise results. Theoretical and experimental power losses are in good agreement. At a conductor current ranging from 650 A to 950 A (rms), specific single-phase losses amount to 1 – 3 W/m. For a three-phase conductor system, specific losses amount to 2.5 – 7.5 W/m. Compared to classical superconducting cables (e.g. Ampacity), the permissible conductor current is smaller by a factor of 4 at identical AC losses. Single-phase specific losses of the single-phase and three-phase set-ups are about the same within the range of measurement uncertainty. Moreover, specific power losses as a function of the cryostat diameter are about the same due to measurement uncertainty. Specific losses are higher for the three-phase set-up with and without a corrugated stainless steel pipe. This increase amounts to about 1 W/m for the measured conductor current of 950 A.

Compared to the concentric conductor concept, the CrossConductor concept is associated with higher losses and, in case losses shall be kept constant, with smaller permissible conductor currents. In comparison to concentric cable design, the outer cable diameter is reduced by the factor by 2. Only the concrete cable system, i.e. line length, permanent current, peak current and allowable AC losses, will decide on the applicability of the CroCo design.

References

- [1] Kottonau, D.; Sousa, W.; Bock, J.; Noe, M.: Design Comparisons of Concentric Three-phase HTS Cables. In IEEE Transactions on Applied Superconductivity, Vol. 29, Issue 6, Sept. 2019, <https://doi.org/10.1109/TASC.2019.2897893>
- [2] Elschner, E; et. al.: New Experimental Method for Investigating AC-losses in Concentric HTS Power. In IEEE Transactions on Applied Superconductivity, Vol. 25, No 3, June 2015, <https://doi.org/10.1109/TASC.2014.2366373>
- [3] Wolf, M.; Fietz, W.; Bayer, C.; Schlachter, S.; Heller, R.; Weiss, K.; HTS CroCo: A Stacked HTS Conductor Optimized for High Currents and Long-Length Production. In IEEE

- Transactions on Applied Superconductivity, Vol. 26, No. 2, March 2016,
<https://doi.org/10.1109/TASC.2016.2521323>
- [4] Preuss, A.; et. al.: Production and Characterization of Strands for a 35 kA HTS DC Cable Demonstrator. In IEEE Transactions on Applied Superconductivity, Vol. 29, No.5, August 2019, <https://doi.org/10.1109/TASC.2019.2909208>
- [5] Gömöry, F.; Vojenciak, M.; Solovyov, M.; Souc, J.: AC losses in coated conductors. In Superconductor Science and Technology, Vol. 23, No. 3, February 2010, <https://doi.org/10.1088/0953-2048/23/3/034012>
- [6] Pham, Q.: Elektromechanische Untersuchungen an REBCO Hochtemperatursupraleitern, Bachelorarbeit, Institut für Technische Physik, REM Bilder Messungen, November 2017.
- [7] Wolf, M.; Bayer, C.; Fietz, W.: Progress in HTS CrossConductor (HTS CroCo) fabrication and characterization. In MEM Workshop, Tallahassee, March 2016, https://nationalmaglab.org/images/news_events/events/mem/talks/s2_wolf.pdf
- [8] Kottonau, D.; Shabagin, E.; Noe, M.; Grohmann, S.: Opportunities for High-Voltage AC Superconducting Cables as Part of New Long-Distance Transmission Lines. In IEEE Transactions on Applied Superconductivity Vol. 27, No. 4, June 2017, <https://doi.org/10.1109/TASC.2017.2652856>
- [9] DIN EN 10380 - Rohrleitungen gewellte Metallschläuche und Metallschlauchleitungen, Deutsche Fassung EN, 2012
- [10] Shen, B.; Coombs, T.; Grilli, F.: Investigation of AC Loss in HTS Cross-Conductor Cables for Electrical Power Transmission. In IEEE Transactions on Applied Superconductivity, Vol. 29, Issue 2, March 2019, <https://doi.org/10.1109/TASC.2018.2881491>
- [11] Norris, T.: Calculation of hysteresis losses in hard superconductors carrying ac isolated conductors and edges of thin sheets. In Journal of Physics D: Applied Physics, Vol. 3, No. 4, Pages 489-507, May 1970, <https://doi.org/10.1088/0022-3727/3/4/308>